Thermal convection in granular gases with dissipative lateral walls

Giorgio Pontuale[1], Andrea Gnoli[1], Francisco Vega Reyes[1,2], and Andrea Puglisi[1]
[1] *Istituto dei Sistemi Complessi - CNR and Dipartimento di Fisica, Università di Roma Sapienza, P.le Aldo Moro 2, 00185, Rome, Italy*
[2] *Departamento de Física and Instituto de Computación Científica Avanzada (ICCAEx), Universidad de Extremadura, 06071 Badajoz, Spain*
(Dated: August 24, 2016)

We consider a granular gas under the action of gravity, fluidized by a vibrating base. We show that a horizontal temperature gradient, here induced by limiting dissipative lateral walls (DLW), leads always to a granular thermal convection (DLW-TC) that is essentially different from ordinary bulk-buoyancy-driven convection (BBD-TC). In an experiment where BBD-TC is inhibited, by reducing gravity with an inclined plane, we always observe a DLW-TC cell next to each lateral wall. Such a cell squeezes towards the nearest wall as the gravity and/or the number of grains increase. Molecular dynamics simulations reproduce the experimental results and indicate that at large gravity or number of grains the DLW-TC is barely detectable.

arXiv:1605.02924v2 [cond-mat.soft] 23 Aug 2016

Shaken granular media escape most of the laws of equilibrium thermodynamics and statistical mechanics [1], ranging from slow plastic flows [2] to fast gas-like dynamics [3–5]. In the wide granular phenomenology [6], an ubiquitous pattern is the convective cell. Notwithstanding its widespread occurrence, many different mechanisms lead to granular convection, and their relevance depends on the granular state under scrutiny.

At high packing fraction and low fluidization, "dense convection" is observed [7–10]. A convincing explanation of dense convection comes from the asymmetric tangential friction at the lateral walls that results in a net downward shear force [11–13]. Dense granular convection can also involve more complex mechanisms, including the formation of unstable heaps at the free surface [14].

In highly fluidized states (granular gases), the only known theoretical mechanism is bulk buoyancy-driven thermal convection (BBD-TC), first observed in simulations [15, 16]. In analogy to molecular liquids [17, 18], it originates from the buoyancy force associated to temperature/density gradients that, because of the intrinsic bulk inelasticity, emerge spontaneously [19], even with an open or reflecting top boundary [20]. BBD-TC is an instability of the hydrostatic state which requires a combination of parameters (including inelasticity, gravity and dimensions) to overcome a certain threshold [21, 22]. A further confirmation that BBD-TC is essentially a "bulk" effect comes from simulations [15] and theory [21, 22] where lateral walls are not required to observe it. Convective circulation in granular gases has been seen also in experiments, where lateral walls are always inelastic [23–26], and successive simulations with elastic [27] and also inelastic walls [28].

The role of lateral walls in dilute granular convection has not been fully understood yet. Some of the mentioned studies recognize that lateral walls influence the observations. For instance, a downward flow velocity is always observed near lateral walls, perhaps because of a reduced buoyancy originated from enhanced dissipation [15, 23, 28]. However, quite contrasting results emerge in simulations and experiments concerning the *necessity* of dissipation at the lateral walls. In some simulations convection is strong even with elastic lateral walls [15], and in some experiments the threshold for convection compares fairly well with theories where lateral walls are absent [25]. In other cases, convection is almost completely killed when wall inelasticity goes to zero, a scenario - incompatible with BBD-TC theories - seen both in simulations [28] and in experiments [26]. Such discrepancies suggest that BBD-TC is not the only mechanism able to generate convection in granular gases. Here we provide the evidence for TC in granular gases induced by dissipative lateral walls (DLW). We employ an ad-hoc experimental setup, able to isolate DLW-TC from BBD-TC, together with molecular dynamics (MD) simulations.

Before introducing our experimental setup, we discuss a general argument in favor of the existence of DLW-TC in *any* vertically vibrated granular system. Let us consider a 2D low density gas (our analysis can be generalized to 3D systems) of identical solid disks of mass m enclosed by two inelastic parallel walls. Perpendicular to the lateral walls, the bottom wall provides energy to the system, for instance through steady vibration or (in numerics) in the form of a thermostat. The system can be considered closed by a fourth upper wall, or open: this does not change our conclusion. A constant gravity field g is acting downwards along the vertical (y) direction. For a dilute granular gas, $p = nT$ (with p the pressure, n the number density, and T the granular temperature) [3]. An outgoing energy flux is always originated at a dissipative wall [29], yielding in our case $\partial T/\partial x \neq 0$ at the lateral walls. We wonder if such a gradient is compatible with hydrostatics, whose momentum balance reads

$$\partial_x p = \partial_x(n(x,y)T(x,y)) = 0 \tag{1a}$$

$$\partial_y p = \partial_y(n(x,y)T(x,y)) = -mgn(x,y). \tag{1b}$$

According to the first equation $p(x,y) \equiv p(y)$, which,

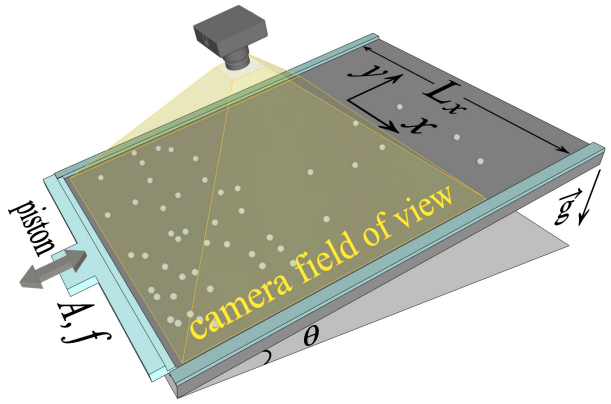

Figure 1. Sketch of the experimental setup. The real length (along y) of the inclined plane, $L_y \gg L_x$, is not marked as it is not essential in the description of the system.

used in the second equation, forces $n(x, y) \equiv n(y)$ and also $T(x, y) \equiv T(y)$. However, this contradicts the necessity of a horizontal temperature gradient induced by DLW. Thus, in the system described any steady state must have flow (that is, a macroscopic velocity field $u \neq 0$) and, since the system is closed in the horizontal, the flow will be convective.

Inspired by such a straightforward observation, we have set up a granular gas experiment under low-gravity, sketched in Fig. 1 and detailed in Supplemental Material [30]. In theoretical studies [21, 22] it is seen that when $g \to 0$ the BBD-TC instability requires a larger and larger wavelength to develop: therefore at a given width of the system there is a gravity value under which unstable perturbations cannot appear and the BBD-TC is suppressed. Our setup is a gas of N spherical steel beads (diameter $d = 1$ mm) moving inside a cuboid of dimensions $L_x = 175$ mm, $L_y = 600$ mm and $L_z = 1.5$ mm $= 1.5d$, thus assuring for a quasi-2D dynamics restricted to the xy plane. This plane has a tilt angle θ with respect to the horizontal: the spheres therefore move with an effective value of gravity $g_{eff} \approx (5/7)g\sin(\theta)$, where g is Earth's gravity acceleration and the constant $5/7$ is due to the moment of inertia of spheres (at the chosen values of θ our trajectories are dominated by pure rolling, see also [31]). The limits of the plane consist of two lateral "walls" made of polycarbonate (at $x = \pm L_x/2$), one inferior wall (at $y = 0$) consisting of a vibrating Plexiglas® piston, and a far top side which is also made of polycarbonate at $y = L_y$. The bottom plate (area $L_x \times L_y$) is made of aluminum alloy and finally the system is covered with a glass plate. The piston oscillates with amplitude A and frequency f. The average squared velocity of the piston, here defined as $v_0^2 = (A2\pi f)^2/2$, helps setting the energy and velocity units in the following. Our setup is similar to that of previous experiments [32, 33] and is of the kind described by eqs. (1). It is worth noting that here, contrary to more common vertical setups [23–26], we can reduce and control the effective gravity. A high speed camera records square images of size $L_x \times L_x$ starting from the maximum position of the piston, i.e. excluding the topmost very dilute region. A pairwise acquisition protocol (see [30]) allows us to reconstruct the average fields $u(x, t)$, $n(x, t)$ and $T(x, t)$ (flow velocity, particle density, and granular temperature, as usually defined [4]) in the visible field, with a a 40×40 mesh. A preliminary study of non-interacting trajectories has confirmed the value of g_{eff} and has shown the presence of small frictional effects in the form of both Coulomb-like friction and viscous-like frictions [30]. We used $N \in [100, 1500]$, which yields an average 2D packing fraction $\nu_{2D} = N\pi(d/2)^2/(L_x L_y)$ in the range of $\nu_{2D} \in [0.1\%, 1\%]$, with observed local variations reaching up to $\sim 5\%$ at the highest values of N and g_{eff}: in summary, we are always in the dilute regime. A detailed assessment of mean free paths measured in the system is discussed in [30]. The amplitude of vibration has been fixed to $A = 1.85$ mm, while the frequency is varied in the range $f \in [10, 45]$ Hz. The inclination angle is varied in the range $\theta \in [0.011, 0.130]$ radiants. Explored values of the rescaled maximum acceleration are $\Gamma = A(2\pi f)^2/g_{eff} \in [70, 3800]$.

Let us discuss our experimental results. In all performed experiments, with an exception discussed below, we always observed convection with two convective cells that span the full width of the 2D plane. Examples of the experimental 2D velocity fields are shown in the top row of Fig. 2. In the special case $N = 100$ we have not observed convection. This may be due to fact that the mean free path is larger than L_x (Knudsen gas) and a consequent possible breakdown of the ideal gas equation of state. In the lower graphs of Fig. 2 we show the experimental hydrodynamic 2D fields for density and temperature. The fields clearly display gradients in both x and y directions. The temperature field (blue-red graphs in Fig. 2) tends to decrease when moving along x from the center to the lateral boundaries as expected from the simple argument of an outward energy flow due to DLW. Along y, the granular temperature shows a richer behavior: for low N and g_{eff} the temperature is dominated by a negative gradient. This would be associated with heat transport from the bottom thermostat to the upmost cold region, where energy is continuously dissipated by inelastic particle-particle and DLW-particle collisions. At larger N and g_{eff} a temperature minimum is observed along y, which can be explained by granular hydrodynamics taking into account a *secondary* energy flux which is associated with the density gradient [34, 35]. The density field (black-yellow graphs in Fig. 2) displays a saddle-like structure. On a horizontal line it shows its largest values near the two DLW ($x = \pm L_x/2$) and a minimum halfway, i.e. at $x = 0$. This is consistent with the fact that particle-wall inelastic collisions favor condensation near the walls. Along the y direction, on the contrary, the density shows a maximum at some given

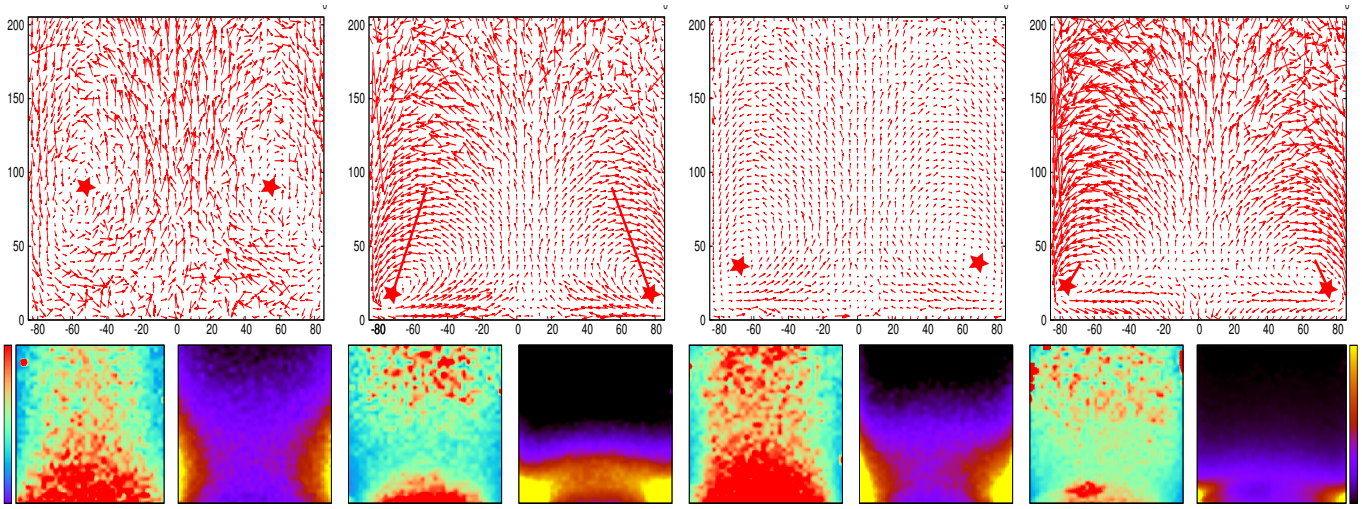

Figure 2. Fields from four experiments with $f = 45$ Hz, $A = 1.85$ mm ($v_0 = 370$ mm/s) and different values of N and g_{eff}. Top row: the velocity field with the two convective cells; coordinates are given in units of particle's diameters (= 1 mm); the center of each cell is marked by a star; in graphs B and D a thick line represents the movement of the cell's center with respect to case A and C respectively. Bottom row: each couple of graphs show the (mass-free) temperature T/m (left) and local packing fraction $\nu = n\pi(d/2)^2$ (right) fields corresponding to the case in the top row. The T scale (see legend on the left) goes from black (colder) at $T = 0$ to red (hotter) at $T = T_{max}$. The ν scale goes from black (more dilute) at $\nu = \nu_{min}$ to yellow (denser) at $\nu = \nu_{max}$. Values of T_{max}/mv_0^2 are: A) 0.2, B) 0.1, C) 0.2, D) 0.4. Ranges for (ν_{min}, ν_{max}) are: A) $(0.02\%, 0.15\%)$, B) $(0.02\%, 0.15\%)$, C) $(0.04\%, 0.1\%)$, D) $(0.005\%, 0.5\%)$.

height. Such a maximum shifts toward the base as N or g_{eff} increase, a fact that is consistent with the increase of steepness in the decay of temperature in the lowest region of the gas. A key observation concerns the behavior of the center of the convective cells: they appear to move toward the lowest corners when N or g_{eff} are increased, as highlighted by the stars superimposed to the velocity fields in Fig. 2B and 2D. Variations occurring when N is increased (decreased) are qualitatively similar to those occurring when g_{eff} is increased (decreased).

How do our observations compare with previous studies? It is likely that experiments in [26] and simulations in [28] were dominated by DLW-TC, as comparison of those results with our Figures 3 and 4 (below) demonstrate. Both cases concern 3D systems, but our argument after Eq. (1) is not affected by a third dimension. In [24] it has been shown that in a dilute granular fluid under vertical vibration, convection takes place only in a limited region of parameter space, at variance with our general argument showing that DLW-TC should always be observed. Our conjecture is that for larger and larger g_{eff} (or N) the two DLW-TC cells occupy a smaller and smaller region of the system, up to a point where the DLW-TC cell is so tiny that it could go unnoticed. As a matter of fact, all experiments in [24] are performed at Earth's gravity, which is much larger than our g_{eff}.

Since our setup has physical limits which prevent θ to become too large, we have performed MD simulations in order to deepen our study and check our previous conjectures. We simulate, by means of an event-driven algorithm a system equivalent to the experimental ones with N *smooth* disks moving in a plane with DLW, gravity acting along $-y$, a thermostat (at temperature v_0^2) at the bottom wall and a topmost wall which has the same inelasticity as the lateral walls, see [30] for details. The collisions between disks are treated with a normal restitution coefficient α, while the disk-wall interactions occur with a normal restitution coefficient α_w (no tangential dissipation is taken into account). We have also checked that friction with the plate and rotations/roughness of disks do not change in a significant way the outcomes of the simulation, confirming that they do not play a relevant role also in the experiment. In Fig. 3A we display an example of results from MD with parameters similar to the experimental setup. The comparison is very good in the shape of convection cells as well as in the density and temperature fields. Performing simulations with many values of all the parameters we confirmed that convection is always present, excluding the very dilute Knudsen-gas regime, where the mean free path is larger than the system lateral size (exactly like in the extremely dilute experiments). Fig. 3B shows that as soon as the lateral walls become elastic ($\alpha_w = 1$) the convective cells disappear and the density/temperature fields become homogeneous along x. Again, this confirms the nature of the convective phenomena that we are observing, as well as the fact that BBD-TC is not acting in our system because of low gravity [21, 22] . Further evidence comes from simulations at increasing system's width L_x, while keeping fixed all the other parameters, as well as N/L_x.

An example of the results is displayed in Fig. 4A. When the width is increased, it appears that the cells have an intrinsic horizontal size L_c because when $L_x > 2L_c$ a *convection-free space* emerges in between. In fact, this region can be identified with the bulk of the fluid, the existence of this region being consistent with predictions from theories without DLW at low gravity [21, 22]. On the contrary, when $L_x < 2L_c$ (as in our experiment), the two cells squeeze in the available space. Figures 4B-E show the behavior of the width of the convection cell and of the intensity of convection (see [30] for definitions) as a function of α_w and of gravity g_{eff}. Two major observations emerge: 1) the intensity of convection decreases linearly with α_w, in a way similar to the observation of [26]; 2) the width of the convective cell decreases when g_{eff} increases. When $g_{eff} \sim g$ convection is barely visible: this can explain the results and the phase diagram described in [24]. In [30] we also show a few more results from MD where density is increased up to a point where BBD-TC also appears, independently of α_w.

The simulations allowed us to verify also cases with DLW ($\alpha_w < 1$) but with $\alpha = 1$: the results appear identical to the results with $\alpha < 1$, indicating that the elastic limit is smooth and that DLW are sufficient to create not only the horizontal gradient but also the vertical ones and drive the system into DLW-TC regime. An approximate estimate of the width of the convection zone from the Boussinesq equation with dissipative lateral walls [36] yields a dependence on α_w and g_{eff} which is in fair qualitative agreement with our observations. The analysis confirms that buoyancy is involved in the DLW-TC mechanism.

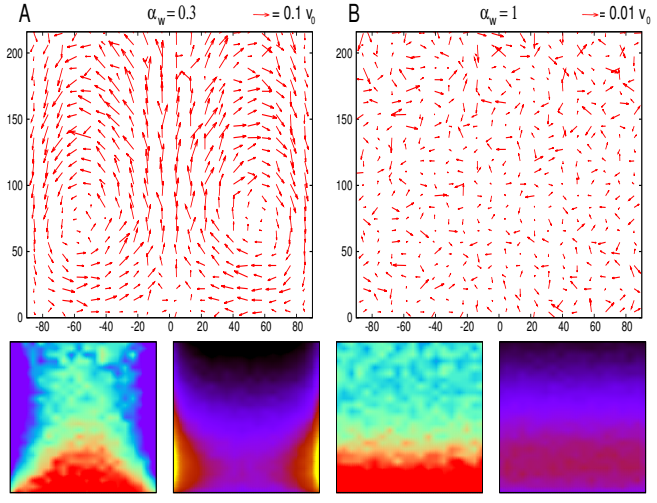

Figure 3. Fields from two simulations with $N = 500$, $g_{eff} = 0.016g$, $\alpha = 0.98$, $v_0 = 280$ mm/s and different values of α_w: in A $\alpha_w = 0.3$, in B $\alpha_w = 1$ (elastic walls). Coordinates and colors are the same as in Fig. 2 with the following values of T_{max}/mv_0^2: A) 0.1, B) 0.2; and the following ranges for (ν_{min}, ν_{max}): A) $(0.05\%, 0.5\%)$, B) $(0.05\%, 0.5\%)$.

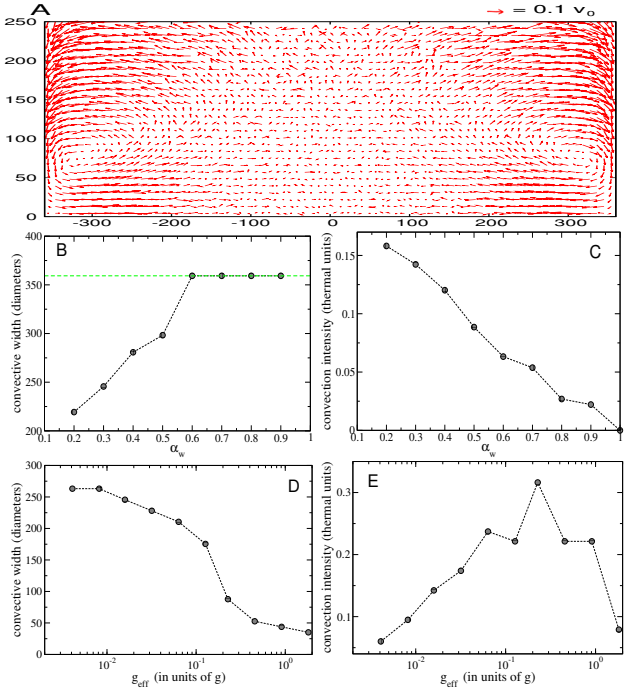

Figure 4. A: velocity field of a large system ($L_x = 720$ diameters) with $N = 2000$, $v_0 = 280$ mm/s, $\alpha = 0.98$, $\alpha_w = 0.3$, and $g_{eff} = 0.016g$. B and C: width and intensity, respectively, of convection as a function of α_w with $g_{eff} = 0.016g$. D and E: width and intensity, respectively, of convection as a function of g_{eff} with $\alpha_w = 0.3$. In graphs B-E we used $L_x = 720$, $N = 2000$, $v_0 = 280$ mm/s, $\alpha = 0.98$.

In conclusion we have demonstrated the existence, for granular gases, of a convective phase induced only by DLW, which becomes important under low gravity conditions. Coupled horizontal and vertical gradients, of both temperature and density, distinguish the TC studied here from that analyzed in previous theories [21, 22] and observed in some experiments [24, 25], where horizontal gradients are absent or irrelevant. The DLW-TC mechanism resembles secondary flows dominated by boundary layer effects and horizontal gradients, such as the tea-leaves paradox [37]. Further theoretical investigation is needed to provide more quantitative predictions from hydrodynamics. New experiments in microgravity are also awaited, as well as possible geophysical applications in low gravity planets, moons and asteroids. We remark that, according to Eqs. (1), convection appears whatever is the magnitude (i.e. no threshold for convection onset) and origin of the horizontal thermal gradient, suggesting a broad validity also outside of the realm of granular fluids.

We wish to thank MD Deen and R. Scaccia for help with the experimental setup, A. Lasanta Becerra for useful discussions and suggestions and A. Santos for a careful reading of the manuscript. F. V. R. acknowledges support from grant "Salvador Madariaga"

No. PRX14/00137 and project No. FIS2013-42840-P (both from Spanish Government) and through project No. GR15104 (Regional Government of Extremadura, Spain, partially financed by the European Regional Development Fund, ERDF).

SM: SUPPLEMENTAL MATERIAL

DETAILS OF THE EXPERIMENTAL SETUP

Our experimental setup consists in a granular partial monolayer moving on an inclined plane and fluidized by the action of a vibrating piston. We refer to Fig. 1 of the Letter for a visual sketch of the setup.

N steels spheres (diameter $d = 1$ mm, mass $m = 4.3$ mg) move, rolling and sliding, on top of a plate made of aluminum alloy which is inclined by an angle θ with respect to the horizontal. The part of the plate where spheres move upon is a rectangular area of dimensions $L_x \times L_y$, with $L_x = 175$ mm and $L_y = 600$ mm. This area is delimited by four "walls": three of them (we call them top, left and right) are at rest, while the fourth (the "bottom") is a vibrating piston. The three walls are made of polycarbonate while the piston is a Plexiglas® slab. The piston vibrates with an almost harmonic law $y_p(t) \approx Asin(2\pi ft)$ thanks to a crankshaft driven by a dc electric motor. Parallel to the aluminum plate, at a distance smaller than 2 spheres' diameters, $L_z = 1.5$ mm, we have placed a transparent "roof" made of thin glass. Particular care has been taken in order to discharge electrostatics, by planting many copper cables in the interior of the plate (from below), all of them connected to a large metal mass (the optical table where the experiment is mounted on). The use of glass for the top cover has improved (with respect to Plexiglas®) the removal of electrostatic charges.

A high speed camera (Photron Mini Ux50) records images (parallel to the plate) of width L_x and height $1.2 \times L_x < L_y$ with minimum ordinate corresponding to the maximum position of the piston, i.e. excluding the topmost region of the system which is indeed very dilute. The image acquisition follows a pairwise protocol: two close frames (at a distance of 0.002 s) are recorded, then 2 seconds are awaited and the cycle is repeated. The two close frames allow to determine the position and velocity vectors $\mathbf{x}_i(t), \mathbf{v}_i(t)$ of the spheres $i \in [1, N]$ (of course it is not guaranteed that in each frame all particles are recognized and tracked). The choice of the time intervals is optimized in order to fulfill the following criteria: the two frames in a pair must be close enough to catch a ballistic (i.e. non-colliding) trajectory, most of the time; the two frames in a pair cannot be too close otherwise image noise cannot be distinguished from real movement; the interval between two pairs of frames must be large enough to improve statistical independence. The methods for locating particles and reconstruct their velocities have been described in previous references [38].

STUDY OF SINGLE PARTICLE DYNAMICS IN THE EXPERIMENT (EVALUATION OF PARTICLE-PLATE FRICTION EFFECTS)

A preliminary study of the single particle (non-interacting) trajectories in the experiment has confirmed that the motion in the xy plane of the center of mass of a particle obeys the following equation:

$$\ddot{\mathbf{r}}(t) = -g_{eff}\hat{\mathbf{y}} - \gamma\dot{\mathbf{r}}(t) - \mu\frac{\dot{\mathbf{r}}(t)}{|\dot{\mathbf{r}}(t)|} \tag{2}$$

with effective gravity $g_{eff} \approx 5/7\sin(\theta)g$ (where g is the normal acceleration of gravity on Earth), viscous coefficient $\gamma = (1.2 \pm 0.4)s^{-1}$ and Coulomb-like (sliding) friction coefficient $\mu = (80 \pm 20)\ mm/s^2$. We have also observed that in the rising part of each trajectory ($\dot{y} > 0$), which usually has a larger initial velocity (after a collision with the energetic piston), viscosity is lower and Coulomb friction is larger, while the opposite occurs in the falling part. This could be due to different modes of motion, e.g. sliding versus rolling. Since it is impossible, with the present setup, to retrieve information about the rotational motion of each sphere, we cannot investigate experimentally this issue. We notice however that the factor $\approx 5/7$ in g_{eff} indicates that the trajectories are dominated by pure rolling.

In the simulations, we have verified that using the real values of μ and γ or putting $\mu = \gamma = 0$ does not change the qualitative picture discussed in the Letter. Quantitatively, the hydrodynamic fields are affected by those values in a way which we do not consider significant.

DEFINITION OF QUANTITATIVE MEASUREMENTS IN EXPERIMENTS AND SIMULATIONS

The system (real or simulated) after a very short transient is in a stationary state and therefore, once the 2D-vectorial positions and velocities of the particles $\mathbf{x}_i(t), \mathbf{v}_i(t)$ are known for n_f frames at times $t \in [1, n_f]$, the coarse-grained "hydrodynamic" fields can be obtained by the following definitions:

$$n(\mathbf{x}_k) = \frac{1}{n_f}\frac{1}{||B_k||}\sum_{t=1}^{n_f}\sum_{i:\mathbf{x}_i(t)\in B_k} 1 \tag{3}$$

$$\mathbf{u}(\mathbf{x}_k) = \frac{1}{n_f}\frac{1}{n(\mathbf{x}_k)||B_k||}\sum_{t=1}^{n_f}\sum_{i:\mathbf{x}_i(t)\in B_k} \mathbf{v}_i(t) \tag{4}$$

$$T(\mathbf{x}_k) = \frac{1}{n_f}\frac{1}{n(\mathbf{x}_k)||B_k||}\sum_{t=1}^{n_f}\sum_{i:\mathbf{x}_i(t)\in B_k} \frac{|\mathbf{v}_i(t) - \mathbf{u}(\mathbf{x}_k, t)|^2}{2}, \tag{5}$$

where $\mathbf{x}_k$ is the coordinate of the k-th point of the mesh and B_k is the cell of the mesh centered at $\mathbf{x}_k$, whose area we call $||B_k||$. In Fig. 2 (experimental fields) we have used a 40×40 mesh, i.e. $k \in [1, 1600]$. In Fig. 3 (simulations) we have used a 20×20 mesh, while in Fig. 4A (simulation with a large system) we used a 80×20 mesh. In both experiments and simulations we used $n_f = 1090$. Temperature and density fields are shown, in Figs. 2 and 3, through a surface interpolation procedure called "pm3d map" in the *gnuplot* software.

In Fig. 4B-E we have also presented two quantitative characterizations of the convective cells, called "convective width" and "convection intensity". Both quantities are obtained by the following procedure: 1) the center of the convective cell is individuated in the plot of $\mathbf{u}(\mathbf{x}_k)$, in particular its ordinate y_c. 2) the vertical component of the average flow at that ordinate, $u_y(x, y = y_c)$ always presents the following oscillatory behavior : at $x \approx -L_x/2$ it takes its (negative) minimum value u_y^{min}, at $x = x_c$ it goes through zero, then at some larger coordinate it reaches a maximum value u_y^{max} and then (if L_x is large enough to leave space for the bulk non-convective region) it quickly goes to zero, touching it at a point x_0 and finally fluctuating around zero for $x_0 < x < 0$; this pattern, of course, repeats specularly in the right half of the system ($0 < x < L_x/2$); 3) the "convection intensity" is calculated as $u_y^{max} - u_y^{min}$ (in Fig. 4C and 4E it is plotted after being rescaled by v_0); 4) the "convective width" is defined, simply, as the final vanishing point x_0 of the vertical field. In the experiment it is quite difficult to repeat the procedure because the total width L_x constrains the two cells, i.e. there is not a point where $u_y(x, y = y_c)$ goes to zero.

DETAILS OF THE MOLECULAR DYNAMICS SIMULATIONS

We have implemented a Molecular Dynamics simulation with N smooth disks of diameter d moving in a rectangular box of dimensions $L_x \times L_y$. The disks follow Eq. (2) when they are not overlapping. When two disks touch, a momentum-conserving inelastic instantaneous collision occurs with restitution coefficient $\alpha \in [0, 1]$ (where the elastic case is given by $\alpha = 1$) [4]. The same kind of collision occurs when a disk touches the lateral walls at $x = \pm L_x/2$ and the top wall at $y = L_y$, with the difference that a wall is treated as an infinite mass particle. A collision with the bottom wall ($y = 0$) conserves horizontal velocity and totally refreshes the vertical one: the new v_y of the disk is extracted randomly with a distribution $P(v_y) = (v_y/v_0^2)\exp(-v_y^2/(2v_0^2))$ restricted of course to $v_y > 0$, which defines the average energy of the thermostat v_0^2.

As mentioned, for all the choices of physical parameters (N, g_{eff}, v_0 etc.) we have performed simulations both with realistic values of γ and μ and with $\gamma = \mu = 0$, and we have not found substantial differences. In the Letter

we have shown the results with the realistic γ and μ.

EVALUATION OF MEAN FREE PATHS AND KNUDSEN NUMBER IN THE EXPERIMENT AND IN THE SIMULATIONS

Since a systematic theoretical framework for the phenomena discussed in our Letter is still lacking, we have decided to give most of the parameters of both experiments and simulations in raw physical units. In the Figures of the Letter we have used adimensional units (e.g. length is rescaled by diameter, temperature field is rescaled by the piston average energy, etc.) for simplicity, without claiming that those reference scales have any theoretical value.

In this section we discuss possible relevant scales, similar to the one used in a previous work [19], in view of a theoretical approach based upon granular gas-hydrodynamics [4, 5].

The Knudsen number reference scale

In standard kinetic theory of non-uniform gases, a usual choice of length and time reference units is the mean free path and collision frequency [39]. The choice of these units emerges naturally from the collisional frequency prefactors that appear in the collisional integrals associated to the transport coefficients of the gas (either molecular gas or granular gas). At the level of the average fields representation, it is also useful this choice of units since it straightforwardly yields the spatial gradients in terms of a reference Knudsen number.

Mean free path and collision frequency can be measured in a generic reference point at local density n_r and local temperature T_r [39] using the following formula valid in dimension $2D$:

$$\lambda_r = (\sqrt{2\pi} n_r d)^{-1} \,, \tag{6}$$

$$\nu_r = \sqrt{\frac{T_r}{m}} \frac{n_r d}{\sqrt{\pi}} \,. \tag{7}$$

As we said, when ν_r, and λ_r are chosen as time and space reference units, complemented with mass particle m for mass, the spatial gradients $\nabla^{(n)}$ from the balance equations in this representation are of the order $\mathrm{Kn}^{(n)}$ which is specially useful since kinetic theory of non-uniform gases is usually developed as a perturbative theory where the distribution function is developed in powers of Kn [40]. The choice of the reference point where granular temperature T_r and density n_r are measured is a subtle question and it may be important to make an optimal choice [41]. In the presence of a gravitational field like in our system we may set our reference point at the bottom piston, since - at least at the theoretical level - temperature and density are constant in its proximity; i.e. we can use $T_r = T(x, y = 0)$ and $n_r = n(x, y = 0)$. A different choice could be more involved since at any other distance y of the piston, temperature and density will also be a function of x due to the dissipative lateral walls (DLW). Due to the complex (non-hydrodynamic) boundary layer problem, each experiment yields different values of $T_r = T(x, y = 0)$ and $n_r = n(x, y = 0)$ and therefore the scaling cannot be anticipated, a real measure of T_r and n_r is necessary. For instance, the rescaled dimensions $\hat{L}_x \equiv L_x/\lambda_r$, $\hat{L}_y \equiv L_y/\lambda_r$, which can be indicated as first estimates of the Knudsen number, are different for each experiment, even if the real size is constant. Some examples of adimensional quantities in the real setup are shown in table I.

N	$\hat{L}_x$	$\hat{L}_y$	$\hat{g}$	$\hat{L}_x\hat{g}$	$\hat{L}_y\hat{g}$
100	0.96	0.96	0.211	0.202	0.693
200	2.19	2.20	0.127	0.277	0.950
300	4.76	4.78	0.086	0.413	1.416
500	14.61	14.64	0.054	0.790	2.709
700	32.72	32.80	0.047	1.549	5.312
1000	76.79	76.98	0.023	1.755	6.018

Table I. Rescaled dimensions and gravity in a series of real experiments with $f = 45$ Hz, $A = 1.85$ mm and $g_{eff} = 0.016\, g$ and different values of N.

The gravity reference scale

A complementary dimensionless representation may be obtained by referring the system size to the length $l_g = v_r^2/g$, with v_r a reference thermal velocity. The thermal velocity is also a non-homogeneous quantity but we can take as a reference its value next to the piston, i.e. for instance $v_r = \sqrt{2T_r/m}$. Of course it is important that the lengthscale induced by gravity is not smaller than the mean free path, i.e. we need a small $\hat{g} \equiv g\lambda_r/v_r^2$. This can be checked in table I.

In table I we give also examples of rescaled length through the gravity reference scale. As we can see in the corresponding values of $L_x/(l_g) = \hat{L}_x\hat{g}$ and $L_y/(l_g) = \hat{L}_y\hat{g}$, they are not too large for all values of N, specially for low N.

TRANSITION TO BUOYANCY-DRIVEN THERMAL CONVECTION

At variance with the DLW-induced convection studied in the Letter, which is always present if $\alpha_w < 1$,

buoyancy-driven thermal convection in granular gases occurs in a limited region of parameters: linear stability of hydrodynamics without lateral boundaries (see Ref. [22] in the Letter) predicts that, at constant gravity and base temperature, it is triggered by an increase of the effective inelasticity $R \propto (1-\alpha)n^2$ where n is the average number density $N/(L_x L_y)$. Moreover, the typical size of the convective cells is predicted to increase with gravity (see Fig. 5 of Ref. [22]).

We have tried to see how buoyancy-driven convection appears in our MD simulations at low gravity. We have chosen a large system (identical to Fig. 4A in the Letter), in order to put in evidence the bulk region which is not affected by boundaries and to enhance the possibility to accommodate bulk-convective cells. Two different situations have been analyzed, one with inelastic lateral boundaries and another one with elastic walls. In both cases, the increase of N (and consequently of R) determines an appearance of buoyancy-driven thermal convection, which is characterized by *many* convective cells spanning the whole width of the system. The following Figure 1 explains the situation:

Below (Figure 2) we report also the plot of the density (packing fraction) field, which is useful to get an idea of the relevance of clustering phenomena: those are expected to play a role when inelasticity or density are large. It is clear that, in the absence of buoyancy-driven convection, there is no clustering (apart from near inelastic walls). The appearance of bulk convection also induces inhomogeneities of the density field, as usual (see for instance Ref. [28] of the Letter).

[1] H. M. Jaeger, S. R. Nagel, and R. P. Behringer, Rev. Mod. Phys. **68**, 1259 (1996).
[2] B. Andreotti, Y. Forterre, and O. Pouliquen, *Granular Media* (Cambridge University Press, 20013).
[3] J. W. Dufty, Adv. Complex Sys. **4**, 397 (2001).
[4] N. V. Brilliantov and T. Pöschel, *Kinetic Theory of Granular Gases* (Oxford University Press, 2004).
[5] A. Puglisi, *Transport and Fluctuations in Granular Fluids* (Springer, 2015).
[6] I. S. Aranson and L. S. Tsimring, Rev. Mod. Phys. **78**, 641 (2006).
[7] C. Laroche, S. Douady, and S. Fauve, J. Phys. **50**, 699 (1989).
[8] J. B. Knight, H. M. Jaeger, and S. R. Nagel, Phys. Rev. Lett. **70**, 3728 (1993).
[9] E. E. Ehrichs, H. M. Jaeger, G. S. Karczmar, J. B. Knight, V. Kuperman, and S. R. Nagel, Science **267**, 1632 (1995).
[10] J. B. Knight, E. E. Ehrichs, V. Kuperman, J. K. Flint, H. M. Jaeger, and S. R. Nagel, Phys. Rev. E **54**, 5726 (1996).
[11] J. A. C. Gallas, H. J. Herrmann, and S. Sokołowski, Phys. Rev. Lett. **69**, 1371 (1992).
[12] J. B. Knight, Phys. Rev. E **55**, 6016 (1997).
[13] E. L. Grossman, Phys. Rev. E **56**, 3290 (1997).
[14] K. M. Aoki, T. Akiyama, Y. Maki, and T. Watanabe, Phys. Rev. E **54**, 874 (1996).
[15] R. Ramírez, D. Risso, and P. Cordero, Phys. Rev. Lett. **85**, 1230 (2000).
[16] P. Sunthar and V. Kumaran, Phys. Rev. E **64**, 041303 (2001).
[17] L. D. Landau and E. M. Lifchitz, *Mécanique des fluides* (Éditions MIR, 1971).
[18] S. Chandrasekhar, *Hydrodynamic and Hydromagnetic Stability* (Dover, New York, 1981).
[19] F. Vega Reyes and J. S. Urbach, J. Fluid Mech. **636**, 279 (2009).
[20] J. J. Brey and D. Cubero, Phys. Rev. E **57**, 2019 (1998).
[21] X. He, B. Meerson, and G. Doolen, Phys. Rev. E **65**, 030301(R) (2002).
[22] E. Khain and B. Meerson, Phys. Rev. E **67**, 021306 (2003).
[23] R. D. Wildman, J. M. Huntley, and D. J. Parkar, Phys. Rev. Lett. **86**, 3304 (2001).
[24] P. Eshuis, K. van der Weele, D. van der Meer, R. Bos, and D. Lohse, Phys. Fluids **19**, 123301 (2007).
[25] P. Eshuis, D. van der Meer, M. Alam, H. J. van Gerner, K. van der Weele, and D. Lohse, Phys. Rev. Lett. **104**, 038001 (2010).
[26] C. R. K. Windows-Yule, N. Rivas, and D. J. Parker, Phys. Rev. Lett. **111**, 038001 (2013).
[27] D. Paolotti, A. Barrat, U. M. B. Marconi, and A. Puglisi, Phys. Rev. E **69**, 061304 (2004).
[28] J. Talbot and P. Viot, Phys. Rev. Lett. **89**, 064301 (2002).
[29] P. R. Nott, M. Alam, K. Agrawal, R. Jackson, and S. Sundaresan, J. Fluid Mech. **397**, 203 (1999).
[30] See Supplemental Material [url], which includes Refs. [38–41].
[31] D. L. Blair and A. Kudrolli, Phys. Rev. E **67**, 041301 (2003).
[32] A. Kudrolli, M. Wolpert, and J. P. Gollub, Phys. Rev. Lett. **78**, 1383 (1997).
[33] A. Kudrolli and J. Henry, Phys. Rev. E **62**, R1489 (2000).
[34] R. Soto, M. Mareschal, and D. Risso, Phys. Rev Lett. **83**, 5003 (1999).
[35] J. J. Brey, M. J. Ruiz-Montero, and F. Moreno, Phys. Rev. E **63**, 061305 (2001).
[36] N. Brilliantov, private communication.
[37] A. Einstein, Naturwissenschaften **14**, 223 (1926).
[38] A. Puglisi, A. Gnoli, G. Gradenigo, A. Sarracino, and D. Villamaina, J. Chem. Phys. **014704**, 136 (2012).
[39] C. Chapman and T. G. Cowling, *The Mathematical Theory of Non-Uniform Gases*, 3rd ed. (Cambridge University Press, Cambridge, 1970).
[40] J. J. Brey, J. W. Dufty, C. S. Kim, and A. Santos, Phys. Rev. E **58**, 4638 (1998).
[41] I. D. Boyd, G. Chen, and G. V. Candler, Phys. Fluids **7**, 210 (1994).

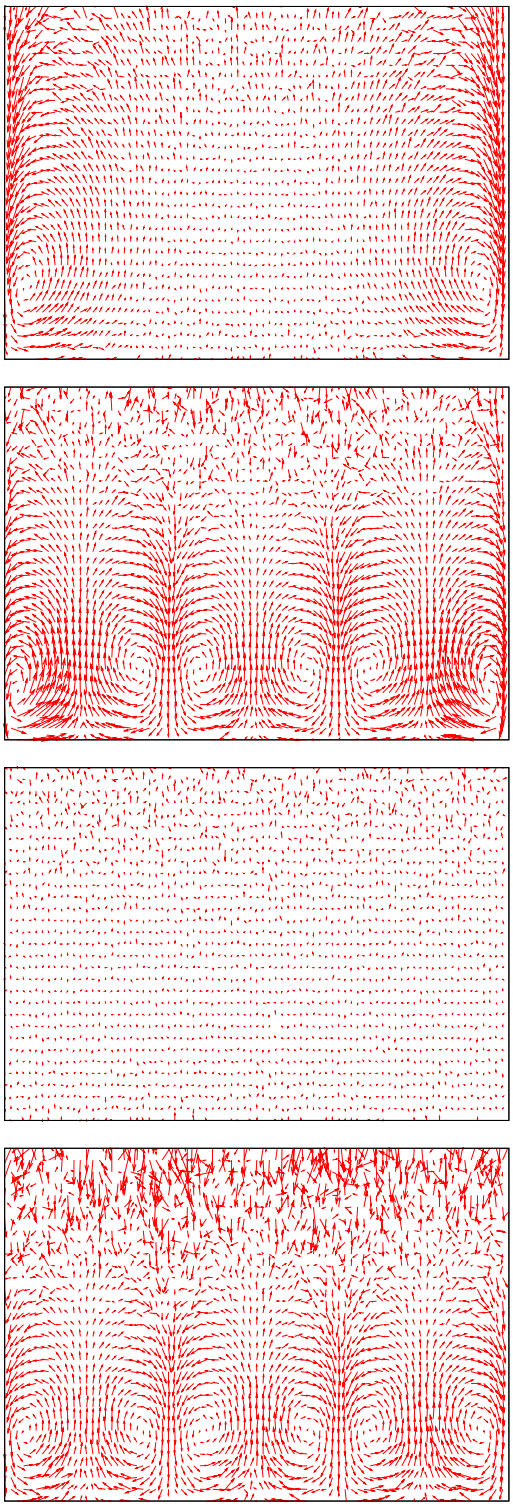

Figure 5. Top left: $N = 2800$, $r_w = 0.3$ (Bulk convection: no. Dlw convection: yes.). Top right: $N = 6000$, $r_w = 0.3$ (Bulk convection: yes. Dlw convection: superimposed.) Bottom left: $N = 2800$, $r_w = 1$ (Bulk convection: no. Dlw convection: no.). Bottom right: $N = 6000$, $r_w = 1$ (Bulk convection: yes. Dlw convection: no.)

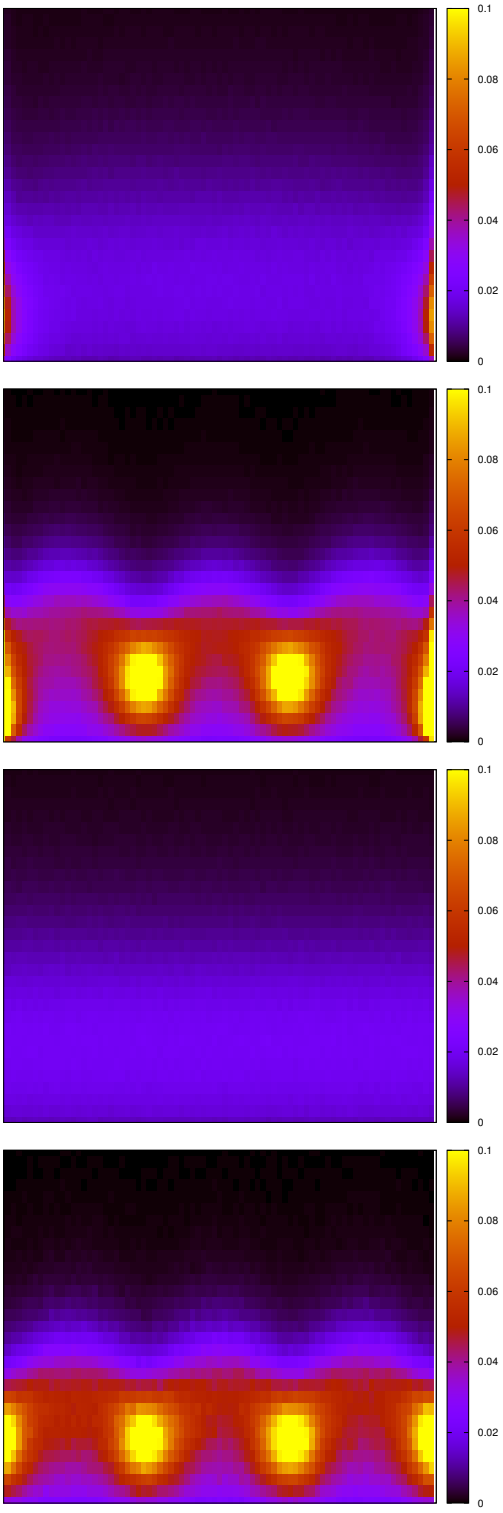

Figure 6. Local packing fraction field. Top left: $N = 2800$, $r_w = 0.3$ (Bulk convection: no. Dlw convection: yes.). Top right: $N = 6000$, $r_w = 0.3$ (Bulk convection: yes. Dlw convection: superimposed.) Bottom left: $N = 2800$, $r_w = 1$ (Bulk convection: no. Dlw convection: no.). Bottom right: $N = 6000$, $r_w = 1$ (Bulk convection: yes. Dlw convection: no.)